Geoderma 337 (2019) 649–663

Contents lists available at ScienceDirect

Geoderma

journal homepage: www.elsevier.com/locate/geoderma

Fingerprinting sediment sources in the water-wind erosion crisscross region on the Chinese Loess Plateau

Jiaqiong Zhang, Mingyi Yang*, Fengbao Zhang, Yuanyuan Li

State Key Laboratory of Soil Erosion and Dryland Farming on the Loess Plateau, Institute of Soil and Water Conservation, Northwest A&F University, Yangling, Shaanxi 712100, China

ARTICLE INFO

Handling Editor: Alex McBratney

Keywords:
Sand sheet
Multiple composite fingerprinting
Sediment source
Wind-water erosion
Climate change

ABSTRACT

Sand sheet sources in the wind-water erosion crisscross region of the Chinese Loess Plateau have not been specifically identified. Spatially, we selected a transect that cuts across the eastern edge of the Mu Us Sandy Land, sand sheets distributed loess hills (sand-loess hills), loess hills, and adjacent rocky mountains to collect surface sediment samples. Temporally, we selected a site on a sampling sand-loess hill to collected depth incremental samples in a 320 cm depth soil profile to analyze sediment sources using the multiple composite fingerprinting approach. We screened out a group of optimal composite fingerprints that correctly classified sediment sources at 100%. Greater than half of all sediment on sand-loess hills originated from the sandy land area on the sampling transect, and roughly half from the sandy land in the soil profile, while the remaining sediment all originated from the loess hills, and rocky mountains had no contributing effect. Coarse particles (> 100 μm) on sand-loess hills were mainly transported from the Mu Us Sandy Land, while fine particles were mainly from loess hills, indicating the importance of aeolian activity in the transport of sand from the Mu Us Sandy Land to loess hills. Environmental changes chronicled by sediment deposition at approximately 12.85 ka BP in the soil profile were primarily attributed to climate change. This study confirms that the composite fingerprinting approach is a feasible method for future studies on sediment sources in areas influenced by complex erosion agencies, landforms and soil types.

1. Introduction

Soil erosion is one of the most severe environmental problems the world is facing today. It significantly contributes to land degradation, as well as a decline in the functional diversity of ecosystems, while also threatening the security of product supplies (Guerra et al., 2017; Pimentel, 2006; Müller-Nedebock and Chaplot, 2015). Sediment tracing, which primarily includes source tracing and yield estimations, is helpful in understanding the transport and redistribution of eroded particles, nutrients and contaminants. It is also useful in revealing geomorphic evolution, understanding interactions between fluvial and aeolian activities, and deducing changes in paleoenvironments and paleoclimates (Haddadchi et al., 2013; Liang et al., 2014; Manjoro et al., 2017; Wang et al., 2017; Williams, 2015; G.J. Zhao et al., 2017; T.Y. Zhao et al., 2017). Sediment research provides evidence for the rational allocation of soil erosion control measures.

To date, sediment source tracing has primarily been studied through surveying, remote sensing, erosion plot observations, simulations, and the fingerprinting technique (Collins and Walling, 2004; Weltje, 2012). Compared to the other approaches mentioned above, the fingerprinting technique is a direct, effective and feasible sediment source tracing approach. Thus, it has been widely used in sediment source studies, and its methodology is being continually improved. The multiple composite fingerprinting approach has replaced the single fingerprinting approach, given that sediment source discrimination have been greatly improved by the former approach (Collins et al., 2017; Gellis and Walling, 2013). Commonly used fingerprinting properties include geochemical elements, radionuclides, isotope, rare earth elements, particle characteristics, magnetic susceptibility, biomarkers, and the concentration of nutrient concentrations (Chen et al., 2017; Hu and Yang, 2016; Gellis and Walling, 2013; Grousset and Biscaye, 2005; Rowntree et al., 2017). The fingerprinting technique also provides a feasible approach for the study of interactions at the interface between ecology and geomorphology (Osterkamp et al., 2012). It has further been successfully applied to trace sources of fluvial and aeolian sediments (Haddadchi et al., 2013; B. Liu et al., 2016; B.L. Liu et al., 2016; Torfstein et al., 2017; Walling, 2013).

Previous studies on fluvial sediment sources have been insightful.

* Corresponding author at: No. 26 Xinong Street, Yangling, Shaanxi 712100, China.
E-mail address: ymyzly@163.com (M. Yang).

https://doi.org/10.1016/j.geoderma.2018.10.024
Received 30 December 2017; Received in revised form 10 October 2018; Accepted 13 October 2018
Available online 22 October 2018
0016-7061/ © 2018 Elsevier B.V. All rights reserved.

Sediment source tracing has expanded from a single erosion event to century scales, and from a catchment to a river basin scales (Collins and Walling, 2002; J.Q. Zhang et al., 2017). Fluvial sediment source studies have clarified the contribution of multiple sources, anatomized the variation of sediment sources in erosion processes, expanded the fingerprinting property dataset, and improved the overall approach (Gellis and Walling, 2013; Haddadchi et al., 2013; Lamba et al., 2015; J.Q. Zhang et al., 2017). Aeolian sediment source studies are more difficult to conduct compared to those related to fluvial activities due to characteristics associate with the multidimensional movement of particles by wind (Field et al., 2009). In previous studies, aeolian sediment source tracing was primarily conducted on large scales such as deserts, continents, or even the planet as a whole, largely based on geochemical elements, while also including properties such as radionuclides, isotope, grain size, and heavy minerals, which is similar to the fingerprinting technique used in fluvial systems (Grousset and Biscaye, 2005; Hu and Yang, 2016; de la Paix et al., 2013; Yang et al., 2007; J.Q. Zhang et al., 2017). Additionally, the geochemical elements-based approach improved our overall understanding of sediment sources. It also provides a basis for the selection of fingerprinting factors. However, geochemical elements-based methods are typically less developed with respect to their methodology compared to the fingerprinting approach. Geochemical elements-based methods are usually based on the distribution, relationship, and proportion between certain typical elements or compounds, while correlation algorithms and models are typically less developed (Grousset and Biscaye, 2005; Gholami et al., 2017).

The exploration of the fingerprinting approach is evolving. Researchers have recognized that fine particle fractions with relatively narrow distribution ranges provide better source discrimination effects. Thus, it has been suggested that a particle fraction of < 10 μm should replace a particle fraction of < 63 μm, which has generally been used in the past. However, this does not mean that a particle fraction of < 10 μm is suitable for all future studies, since larger particle size fractions may be optimal for source discrimination when sediments contain significantly different geological characteristics. Additionally, researchers have emphasized the importance of uncertainty analysis. This is because uncertainty analysis is an essential part of sediment source tracing when using the fingerprinting approach, which could be caused by issues related to source classification, differences in measurement precision of potential fingerprinting factors, preselection procedures of potential fingerprinting factors, and model selection (Collins et al., 2017; Zhang and Liu, 2016; Sherriff et al., 2015).

For the Chinese Loess Plateau (CLP), sediment source studies have explored loess sources from seasonal variation to historical geological records, and from small catchments to whole continents using types of methods previously mentioned. Most researchers believe that sorted loess particles deposited on the CLP were transported from the northeastern region of the Tibetan Plateau by strong winter monsoons, while finer particles were transported to areas further afield, such as Southeast Asian (Nie et al., 2015; Stevens et al., 2013; Wang et al., 2015; F.B. Zhang et al., 2017). On the basis of these studies, it can be deduced that loess deposition on the CLP has primarily been driven by aeolian forces in combination with fluvial redistribution. At the same time, it is reasonable to assume that these loess sources are closely associated with the Mu Us Sandy Land, which is adjacent to the CLP in an upwind direction.

There is a transition zone located between the Mu Us Sandy Land and the Loess Plateau. This specific transition zone is a hilly region with patchy aeolian sand deposits (sand sheets). This zone is typical of the wind-water erosion region, and it is also an area where soil erosion susceptibility has a tendency to be more severe compared to regions of erosion dominated by wind or rainfall alone (Bullard and Livingstone, 2002; Field et al., 2009). This zone is consequently becoming the central area of erosion on the Loess Plateau (Tang et al., 1993). Moreover, eroded soil transported from this transition zone has greatly contributed to the sediment load of the Yellow River, especially when the total sediment load of the river has significantly decreased in recent years (Wang et al., 2016). Thus, it is clear that, in order to control the sediment load of the Yellow River, it is important to improve the ground stability of the transition zone. It is also important to understand where sediment sources originated from in the transition zone, and subsequently taking control measures.

Researchers have hypothesized that sand sheets could have been either transported from the Mu Us Sandy Land by winds or formed by the redistribution of disparate local soils in erosion processes. However, no study has yet been conducted to confirm these assumptions. On the basis of previous studies, it is clear that sediment was transported from a northwest to southeast direction by winter monsoons, and sediment on the Loess Plateau has intrinsically been linked to the Mu Us Sandy Land. In this study, we assumed that the Mu Us Sandy Land and local loess were both potential sources of specific sand formations in the wind-water erosion crisscross region of the CLP. To confirm this hypothesis, we applied the multiple composite fingerprinting approach to clarify sand sheet sources, to estimate the contribution of each source, and to verify the feasibility of the multiple composite fingerprinting approach in tracing sediment sources under a complex environment. Results from this study will be helpful for soil erosion control in this region and also beneficial to decrease sediment loads in the Yellow River.

2. Materials and methods

2.1. Study area

The study area included the eastern edge of the Mu Us Sandy Land, the wind-water erosion crisscross region of the Loess Plateau where the sand sheets are distributed, loess hills devoid of sand deposits, and rocky mountains located in the southeastern region of Shenmu County (Fig. 1a). The eastern edge of the Mu Us Sandy Land is composed of fixed sandy land and dunes (mostly transverse dunes). The sand sheet area is characterized by fragmented loess hills comprised of both aeolian and fluvial landforms, the loess area is composed of hills and gullies devoid of sand deposits; and the rocky mountain area is composed of a very thin soil layer devoid of aeolian sand deposits. According to our investigation, the elevation of the study region ranges from 1272 m AMSL in the northwest to 992 m AMSL in the southeast. This semiarid region is a transition zone that changes from grassland to desert. Local weather is characterized by dramatic interannual variation. Weather data from two meteorological stations in the region (i.e., the Jinjie and Shenmu meteorological stations) recorded an annual average temperature of 7.9 °C with a recorded maximum of 23.6 °C in July and a recorded minimum of −9.7 °C in January. Annual precipitation averages 393.9 mm, most of which (70.2%) falls from June through September. The prevailing wind is from the northwest, with an average velocity of 4.8 m s^{-1}, a maximum of 20 m s^{-1}, and approximately 30 d of gale winds ($\geq$17 m s^{-1}) per year on average. This area is also an agricultural and pastoral transition zone, and land use types are consequently diverse. As a result, this region is sensitive to climate change.

2.2. Transect selection

We selected a sampling transect running lengthwise for approximately 65 km in a northwest to southeast alignment, which includes sandy land, sand-loess areas, loess hills, and rocky mountain areas according to previous research results, assumptions of this study, and local prevailing wind directions. The sampling transect was comprised of 14 sub-transects that included three groups of semifixed sand dunes, three groups of fixed sandy land and dunes, three sand-loess hills, three loess slopes, and two rocky mountains (Fig. 1b). The dune and hilly areas investigated for this study are all aligned in a northwest to southeast direction. Semifixed sand dunes were mainly fixed by living *Artemisia desertorum* (Asteraceae) checkerboards (with an approximate

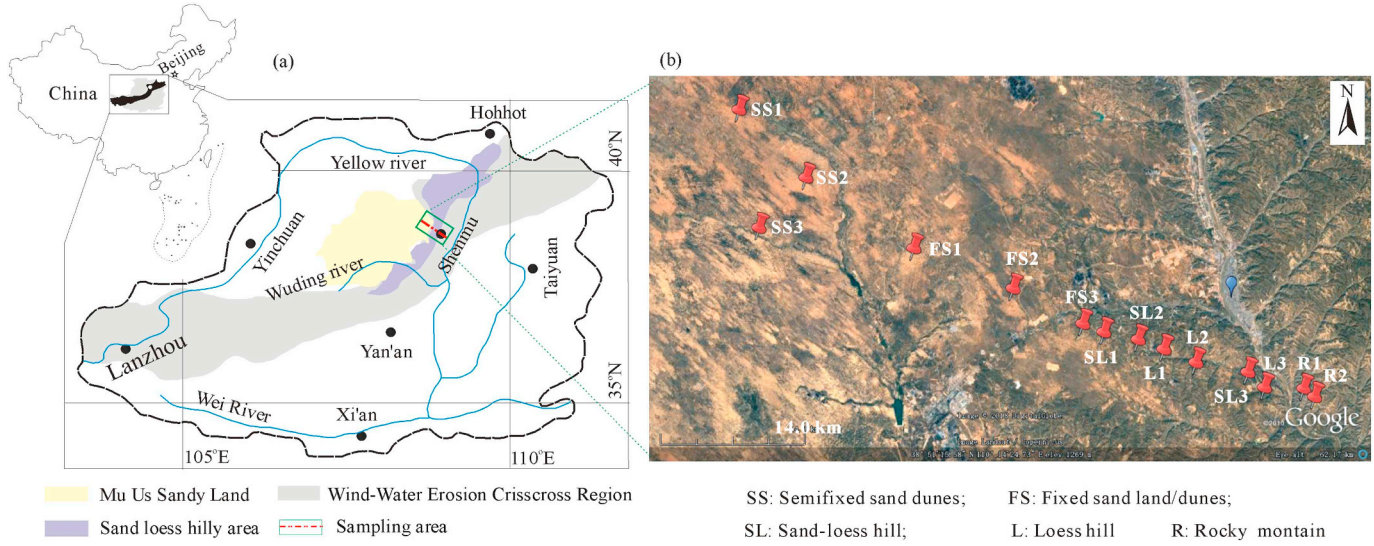

Fig. 1. Location of the study area (a) and the sampling transects (b).

15% CV); the fixed sand area was primarily covered by artificial *Caragana korshinskii* (Leguminosae) and *Salix cheilophila* (Salicaceae) (with an approximate 45% CV); the sand sheet areas of sand-loess hills were mainly covered by *Populus simonii* Carr. (Salicaceae) and *Caragana korshinskii* (Leguminosae); the remaining areas were either cropland or abandoned cropland. These abandoned croplands were typically distributed within areas of high erosion potential, namely, steep sloping fields on loess hills. The "Grain for Green" program established by the Government of China converted cropland into grassland and artificial forest. Moreover, grazing was restricted by government-sanctioned environment protection. The rocky mountains area locating southeast of the loess hills was covered by very thin and discrete soil (< 5 cm by our measurements) with no sand sheets formed. This rocky area is mostly barren, but low grass grows in areas with soil (Fig. 2).

2.3. Sediment sampling

We collected soil samples at a depth from 0 to 5 cm (i.e., topsoil) from most sampling transects based on knowledge gained by previous conducted studies within similar environments (B. Liu et al., 2016; B.L. Liu et al., 2016; G.J. Zhao et al., 2017; T.Y. Zhao et al., 2017). The sampling depth in the rocky mountain area was from 0 cm to the rock surface when the soil depth was < 5 cm. We collected three subsamples in rows approximately 1 m apart and then combined them into one sample for analysis. Sampling sites were arranged based on variation in geomorphology, sediment properties, and the total length of the sampling transect, while we collected more samples in sand sheet areas. For semifixed and fixed sand dunes areas, sampling transects included at least two continuous transverse dunes ranging from 410 to 685 m, where 14 to 18 sampling sites were established. Transects on loess hills averaged 2475 m in length, while transects that crossed hills in the sand-loess hilly area averaged approximately 2430 m, where 27 to 35 sampling sites were established. Transects on the rocky mountain area averaged 684 m, which included approximately 15 sampling sites. We collected 47 samples from the semifixed sand dunes areas, 51 samples from the fixed sand dune areas, 45 samples from loess slopes, 89 samples from sand-loess hills, and 29 samples from the rocky mountain area. In total, we collected 261 samples. Additionally, we chose a site at the southeastern aspect from one of the sampling sand-loess hills (SL2) to collect depth incremental samples. It was selected as a deposition site where water or wind erosion were extremely unlikely to have occurred. Thus, it was located on the leeward slope of local prevailing winds with relatively gentle slope gradient and greater vegetation cover. Sand and loess deposits were observed in a soil profile of 320 cm depth. We collected depth incremental soil samples based on the deposition layers (Fig. 3). The depth interval was approximately 10 cm for most soil samples with the exception of two samples from 290 to 300 cm in the soil profile (the depth interval was 5 cm) depending on visible changes in soil particle size. In total, we collected 33 samples in the soil profile. All samples were collected in June 2015.

2.4. Sample analysis

The preselection of tracers is an important step in sediment tracing. Such preselection is typically based on both the physical environment and previous experience. As stated in previous studies, we agree that there was closely linkage between the Mu Us Sandy Land and the Loess Plateau (Nie et al., 2015; Stevens et al., 2013; Wang et al., 2015). However, their site conditions were obviously different with respect to soil, vegetation, landforms, and land use types. Thus, it is reasonable to preselect factors related to geological properties, since geology was identified as the major controlling factor affecting source group classification (Pulley et al., 2017). Moreover, previous studies conducted in nearby regions or having similar environment conditions indicated that effective discrimination characteristics of sediment sources primarily include magnetic susceptibility, particle characteristics, and geochemical elements (Jia et al., 2011; Liang et al., 2013; Yu et al., 2016; G.J. Zhao et al., 2017; T.Y. Zhao et al., 2017). On the basis of both geological conditions and previous experience, we preselected grain size distribution, magnetic susceptibility, and geochemical elements concentration as potential fingerprinting factors for tests. All samples were air dried, ground with a mortar and pestle, and passed through different sized nylon screens before determining the values of the potential fingerprinting parameters. We determined the particle size distribution of all fine particles (< 2 mm in diameter) using a Mastersizer 2000 particle size analyzer (Malvern Instruments, Malvern, UK), and coarser particles (> 2 mm in diameter) using the weighting method. We measured soil magnetic susceptibility including both high-frequency (χ_{hf}) and low-frequency (χ_{lf}) susceptibilities using the MS2 dual-frequency magnetic susceptibility instrument (Bartington Instruments, Witney, UK). We measured a total of 45 geochemical elements using an inductively coupled plasma mass spectrometry (ICP-MS) after samples were sieved to < 63 μm at the Bureau Veritas Minerals Laboratory (Vancouver Office, British Columbia, Canada). Particle fractions < 63 μm were used in this study according to Collins et al. (2017), who reported that coarse particle size fractions were optimal when sediment

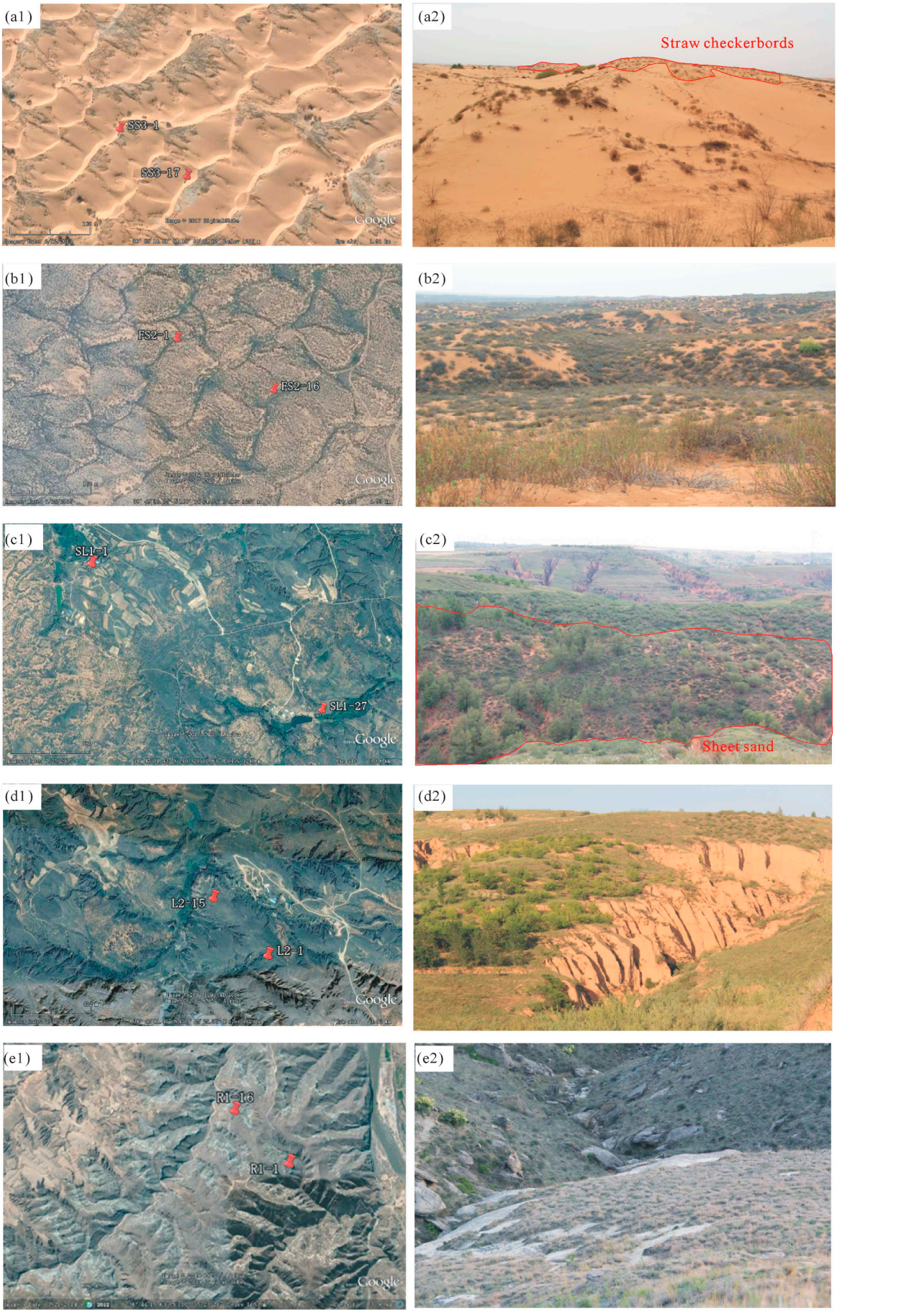

(caption on next page)

Fig. 2. Environmental conditions of sampled semifixed sand dunes (a1 and a2), fixed sandy land and dunes (b1 and b2), sand-loess hills (c1 and c2), and loess hills (d1 and d2) taken from Google Earth (a1–d1) and obtained through a local investigation (a2–d2).

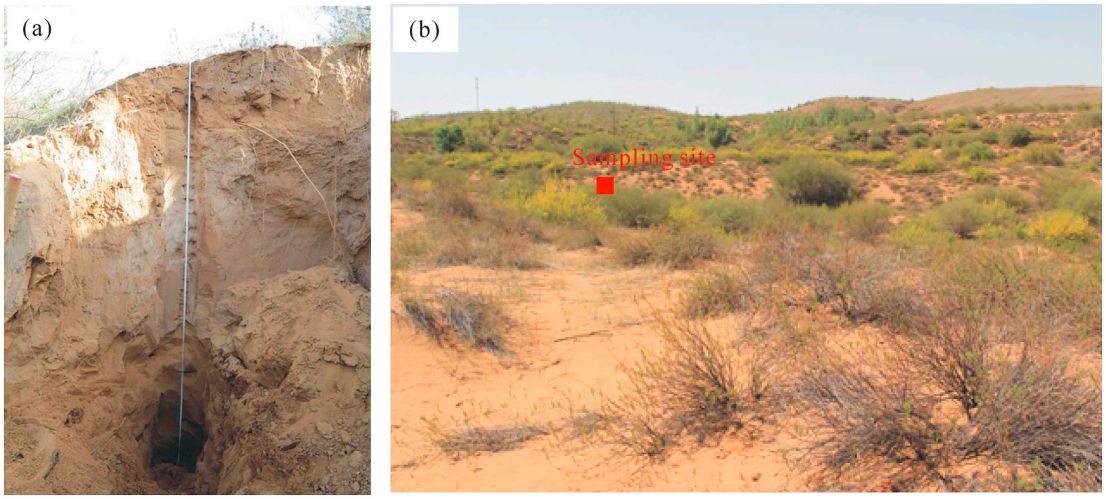

Fig. 3. The soil profile (a) and its surrounding area (b).

sources categorized geological characteristics. Measured geochemical elements included Mo, Cu, Pb, Zn, Ag, Ni, Co, Mn, Fe, As, U, Th, Sr, Cd, Sb, Bi, V, Ca, P, La, Cr, Mg, Ba, Ti, Al, Na, K, W, Zr, Ce, Sn, Y, Nb, Ta, Be, Sc, Li, S, Rb, Hf, In, Re, Se, Te, and Tl. Additionally, depositional years of four loess samples collected from the soil profile were analyzed using radiocarbon dating at Beta Analytic Inc. (Miami office, Florida, USA). Characteristics of particle size were expressed using the mean grain size (M_z). Grain size parameters were calculated using the formulas by Folk and Ward (1957), and the classification of grain size followed the USDA scale (USDA, 1951). Accordingly, we tested a total of 48 potential fingerprinting tracers for this study.

2.5. Sediment source tracing

Sediment sources were traced using the multiple composite fingerprinting approach. This approach is applies screening to establish the optimal combination of fingerprinting properties, and estimates contributions of potential sediment sources using suitable models. Four steps are typically involved in the screening procedure of the optimal fingerprinting properties. The first step is to identify the potential fingerprinting properties from preselected factors using the Kruskal-Wallis *H* test. The second step is to classify meaningful parameters into appropriate categories using discriminant function analysis (DFA), which is a stepwise analysis approach based on Wilks's lambda distribution (Wilk's λ). This step is applied when the Kruskal-Wallis *H* test cannot confirm all potential factors. The third step is to confirm the conservative behavior of fingerprinting factors by means of different types of statistical analyses to ensure their reliability in sediment source discrimination. Reliability analysis typically needs to confirm the conservative behavior of parameters through a comparison analysis of element concentrations between source samples and deposition sediment samples, to ensure that the mean concentration in deposition sediment is within the range of the source mean concentration, and to ensure the distribution consistency between sediment and source samples. Moreover, it is also necessary to exclude factors that could generate higher discriminant uncertainty of sediment sources by conducting statistical tests, such as variability ratios tests (Gellis and Walling, 2013; Koiter et al., 2013; Pulley et al., 2017; Wilkinson et al., 2013). The forth step is to confirm the optimal combination of fingerprinting properties using multivariate discriminant analysis (MDA). Thus, the potential fingerprinting properties must meet following constraint conditions (constrained optimization): detectable parameter concentrations are statistically significant, and they are able to distinguish between potential sediment sources with conservative behavior and relatively low uncertainty. When optimal fingerprinting factors were established through screening, we obtained the contribution of each potential sediment deposit source using a multivariate mixing model (Walling et al., 1999). This model minimizes the sum of the weighted relative square errors in a set of linear equations, and is expressed as follows:

$$f = \sum_{f=1}^{n} \left\{ \left[C_f - \left(\sum_{s=1}^{m} P_s S_{sf} \right) \right] / C_f \right\}^2 \quad (1)$$

where n is the number of fingerprinting factors selected in the optimal combination of fingerprinting factors; C_f is the concentration or value of factor f in the sediment; m is the number of potential sediment sources; P_s is the proportional contribution of sediment from potential source s; and S_{sf} is the average value of factor f in potential source s when all detectable parameters obey the normal distribution according to Q-Q (quantile-quantile) plots using SPSS 19.0. We applied this model under two constraints: the contribution of each source had to be non-negative and contributions sum to 1 (Collins et al., 1997).

Previous studies suggested that the genetic algorithm is one of the most powerful optimization tools to minimize the objective function, and it is able to obtain optimal source contributions to sediment in combination with Monte Carlo analysis (Collins et al., 2010; Haddadchi et al., 2013). This study applied 5000 Monte Carlo iterations as a surrogate for conventional random sampling together with genetic algorithm optimization to obtain accurate prediction contributions. Moreover, uncertainty in source contributions primarily caused by properties of fingerprinting factors and optimization of the mixing model were estimated by incorporating Monte Carlo analysis into the optimization routines of the mixing model. Sample means and the relative standard deviation (SD) of tracers for each potential source were estimated using a bootstrap procedure. This was conducted to infer the statistical distribution of tracers on the basis that analytical errors and variability of tracers based on the sampling regime of each source area could represent the overall source. We applied *t*-tests in this study to analyze the contribution uncertainty of sediment sources (Walling, 2013). Additionally, we tested source apportionment modeling outputs using artificial source material mixtures due to the dependence of source

Table 1
Optimal fingerprinting properties based on discrimination results for adaptability model testing.

Step	Selected fingerprinting property	Cumulative correct classification of the source (%)	Correct classification of the source based on a single fingerprinting property (%)
1	Sr	96.7	96.7
2	M_z	100	100

attributions on the models (Collins et al., 2017). To overcome the problem of using methods as local optimization tools, such as the solver add-in program of Excel is unable to determine the optimum sediment contribution while minimizing the error of the mixing model, we used goodness-of-fit (GOF) analysis. The GOF was assessed by the mean absolute error rather than the more typically used mean relative error, due to the potential risk of estimation bias of the relative error-based GOF (Laceby and Olley, 2015; Manjoro et al., 2017),

$$GOF = \frac{1}{n}\left[1 - \sqrt{\sum_{f=1}^{n}\left(1 - \frac{\sum_{s=1}^{m} x_s a_{fs}}{C_f}\right)}\right] \quad (2)$$

where a_{fs} is the mean concentration of tracer property f in source type s (s = 1 to m), x_s is the unknown relative weighting contribution of source type s to the sediment sample, and C_f is the range of tracer property f in the dataset, which is used to normalize the range of tracer properties. This equation must also satisfy the following constraints (Palazón et al., 2015):

$$C_f = \sum_{s=1}^{m} x_s a_{fs}, \quad (3)$$

$$\sum_{s=1}^{m} x_s = 1 \quad (0 \le x_s \le 1) \quad (4)$$

When the GOF value is > 80%, mixing model estimations are considered satisfactory for the sediment source contributions (Collins et al., 1997; McKinley et al., 2013).

3. Results

Samples collected from the rocky mountain area were removed from our analysis due to the following reasons. First, these samples had little bearing on the formation of sand sheets according to the artificial source material mixture test. Second, some of the fingerprinting parameters in this area were significantly different from the other areas investigated. Taking grain size as an example, a large proportion of the thin soil layer that overlaid the extensive rock formations was composed of the original weathered gravel (grain size > 2 mm), and some rocky mountain sites were even entirely composed of gravel, while there is no such coarse particles in the other sampling areas at all. Third, eroded particles were primarily transported by winter monsoons, which was dominated by northwestern winds. As reported by previous studies (Nie et al., 2015; Stevens et al., 2013), the direction of particle transport was mainly from the northwest to the southeast.

3.1. Testing the source apportionment outputs of the model

Source apportionment modeling outputs were tested using artificial source material mixtures. The preparation and testing of mixed samples were taken from source samples collected from the Mu Us Sandy Land and local loess slopes. We stochastically selected one sample from the samples of each potential source area. They were mixed to create seven groups of proportional artificial mixtures (1:1, 2:3, 1:3, 1:9, 3:2, 3:1, and 9:1) and classified into three types: half mixture (1:1), sand-like sediment (2:3, 1:3, and 1:9) and loess-like sediment (3:2, 3:1, and 9:1). The total sample weight was the same (10.0 g) for all types of proportional artificial mixtures. We generated five duplicates of each proportional type from which to analyze the multivariate mixing model using these 35 artificial mixtures. The procedure used in this study was similar to the procedure used by Haddadchi et al. (2014). Results from the nonparametric Kruskal-Wallis H test showed that parameters were all statistically significant ($P < 0.05$) with the exception of Ca, Cu, Al, Be and Rb as well as the undetectable elements in selected samples (Ag, Cd, Bi, S, In, Re, Se, Te and Tl). Stepwise DFA screened two traces (Sr and M_z) with conservative behavior from the 34 potential tracers that passed the Kruskal-Wallis H test, including Mo, Pb, Zn, Ni, Co, Mn, Fe, As, U, Th, Sr, Sb, V, P, La, Cr, Mg, Ba, Ti, Na, K, W, Zr, Ce, Sn, Y, Nb, Ta, Sc, Li, Hf, χ_{hf}, χ_{lf}, and M_z. The Sr and M_z fingerprint factors successfully assigned 100% of all three types of artificial mixtures to their known sources (Table 1). This meant that the cumulative correct classification of the multivariate mixing model were 100%. Thus, we determined that the source apportionment outputs from the applied multivariate mixing model were acceptable for this study.

3.2. Source discrimination of sand sheets

For samples collected from potential source transects, Ag, S, In, Re, Se and Te were undetectable in almost all samples, while Cd, Bi, and Tl were undetectable in greater than half of the samples. Thus, we removed these nine factors from the analysis. Moreover, we also removed factors when their concentration range in sediment samples were without the range of their source values (Cu, Co, Mn, Fe, Sr, Cd, Ca, P, Cr, Mg, Ba, Al, Sn and Nb), and the mean sediment concentration was beyond the source category mean values (Rb). The mean concentrations of fingerprinting tracers that passed testing were all in the range of the source group mean values. The Kruskal-Wallis H test screened out a non-significant factor Be (Table 2). Stepwise DFA found that the remaining 23 factors differed significantly between potential sources. As a result, they further underwent stepwise DFA. Finally, seven factors comprised of the optimum composite fingerprints, including $\chi_{hf,}$ Zn, Ti, As, Ni, Li and M_z. Furthermore, χ_{hf} was removed from the optimum composite fingerprints even though it passed the DFA test due to its high intergroup variability (i.e., the variable coefficient was > 88% of the fingerprinting factors), which greatly increased the contribution of source uncertainty. Further correspondence analysis was produced using biplots between source and sediment samples on condition that we classified sediments on sand sheet hills into loess (M_z > 3.74 Φ (i.e., < 75 μm)), sand (M_z < 2.32 Φ (i.e., > 200 μm)), and a mixture of both (3.74 Φ ≥ M_z ≥ 2.32 Φ). The classification of particles was based on findings from grain size comparison analysis between sediments and source samples collected from the Mu Us Sandy Land and loess collected from loess hills. Biplots results exhibited a similar linear distribution between sources and sediments for both sand and loess samples, and sand-loess mixture was distributed between them (Fig. 4). Thus, the final optimal composite fingerprints included Zn, Ti, As, Ni, Li, and M_z. These optimum composite fingerprinting factors correctly classified sediment sources with a cumulative correct classification of 100% (Table 3).

3.3. Source apportionment of sand sheets

The GOF ranged from 75.4% to 97.4% and averaged 88.6%. This indicated that the mixing model algorithm approach we adopted provided an acceptable prediction level of source contributions. As a whole, the sediment contribution for the sand sheets on hills transported from the Mu Us Sandy Land was more (56.2% ± 0.4%) compared to local loess (43.8% ± 0.4%). However, sediment sources varied significantly between sampling sites. The sediment contribution of certain sites came entirely from local loess, while that of other sites came entirely from the Mu Us Sandy Land. For the remaining sites,

Table 2
Results of the Kruskal-Wallis *H* test for sediments on sand-loess hills.

Element	MDL	Elements < MDL in source samples (%)	Value in source samples						Value in sediment samples						*H* value	*P* value
			Sand from Mu Us Sandy Land			Loess from loess hills			Sheet sand hills			Soil profile				
			Mean	Max.	Min.	Mean	Max.	Min.	Mean	Max.	Min.	Mean	Max.	Min.		
[b]Mo[d] ppm	0.1	0	4.5	15.1	1	0.7	4.3	0.2	1.6	4.6	0.2	0.3	0.6	< 0.1	101.799	< 0.001*
[ab]Cu ppm	0.1	0	16.2	65.2	6.4	18.6	40.8	6.4	15.1	40.8	3.4	10.6	19.0	2.5	26.549	< 0.001*
[b]Pb ppm	0.1	0	15.5	20.5	12.2	19.2	23.0	14.6	17.5	22.8	13.6	16.5	18.6	12.2	95.580	< 0.001*
Zn ppm	1	0	22	62	10	50	67	24	32	67	15	26	48	11	96.994	< 0.001*
Ag ppm	0.1	97.4	–	–	–	–	–	–	–	–	–	–	–	–		
[b]Ni ppm	0.1	0	8.5	15.1	4.6	25.3	35.1	9.2	14.8	35.1	5.6	13.1	27.0	1.9	111.338	< 0.001*
[ab]Co ppm	0.2	0	3.3	5.3	2.4	9.8	14.4	3.8	5.9	12.3	2.3	5.1	10.0	0.9	114.858	< 0.001*
[ab]Mn ppm	1	0	270	404	169	509	647	237	351	647	137	276	521	44	104.372	< 0.001*
[ab]Fe %	0.01	0	1.56	2.29	1.05	2.47	3.16	1.51	1.86	3.09	0.75	1.39	2.47	0.29	97.540	< 0.001*
As ppm	1	0	3.4	5	1	9.7	14	4	5.9	13	2	5	13	1	116.340	< 0.001*
[b]U ppm	0.1	0	0.5	0.8	0.3	1.5	2.1	0.7	0.9	1.8	0.4	1.0	1.9	0.3	117.067	< 0.001*
[b]Th ppm	0.1	0	2.4	4.1	1.6	9.2	12.2	3.2	5.2	11.1	2	5.5	10.2	1.5	115.759	< 0.001*
[a]Sr ppm	1	0	387	456	320	214	354	153	300	414	138	287	392	176	112.537	< 0.001*
[a]Cd[d] ppm	0.1	66.0	< 0.1	0.2	< 0.1	0.2	0.3	0.1	0.1	0.3	< 0.1	–	–	–	0.255	0.614
Sb ppm	0.1	0	0.3	0.5	0.2	1.1	1.8	0.4	0.6	1.3	0.3	0.6	1.3	0.2	118.758	< 0.001*
Bi ppm	0.1	55.8	< 0.1	0.2	< 0.1	0.2	0.3	0.1	0.2	0.3	0.1	0.2	0.3	0.1	3.036	0.081
[b]V ppm	1	0	20	37	10	61	84	26	37	80	11	38	73	8	114.236	< 0.001*
[ab]Ca %	0.01	0	0.91	1.22	0.65	2.83	7.22	0.92	1.46	5.65	0.46	0.88	1.52	0.38	97.408	< 0.001*
[ab]P %	0.001	0	0.019	0.029	0.011	0.047	0.069	0.022	0.035	0.082	0.014	0.028	0.064	0.008	113.209	< 0.001*
La ppm	0.1	0	12.3	16.7	8.6	28.1	36.3	14.5	19.1	36.3	11.3	20.6	33.1	9.1	114.768	< 0.001*
[ab]Cr ppm	1	0	17.1	30	10	48.9	61	23	32.4	60	10	21	47	3	115.523	< 0.001*
[ab]Mg ppm	0.01	0	0.21	0.35	0.12	0.81	1.20	0.29	0.44	0.97	0.11	0.41	0.84	0.06	115.926	< 0.001*
[a]Ba ppm	1	0	885	1001	777	566	867	428	783	1001	428	776	913	515	107.874	< 0.001*
Ti %	0.001	0	0.132	0.292	0.049	0.306	0.361	0.155	0.217	0.359	0.054	0.201	0.351	0.050	108.027	< 0.001*
[ab]Al[d] %	0.01	0	5.95	6.93	4.98	5.97	6.71	5.15	5.94	7.15	4.30	6.38	8.50	4.16	0.526	0.450
Na %	0.001	0	2.631	3.019	2.203	1.599	2.487	0.645	2.216	2.954	0.925	2.057	2.651	1.373	110.687	< 0.001*
K %	0.01	0	2.54	2.82	2.29	2.02	2.53	1.61	2.35	2.77	1.61	2.36	2.76	1.76	102.392	< 0.001*
W ppm	0.1	0	0.3	0.8	0.2	1.3	1.9	0.5	0.7	1.9	0.3	0.7	1.4	0.2	118.218	< 0.001*
[b]Zr ppm	0.1	0	23.5	35.6	16.7	63.6	85.6	31.2	42.6	72.5	20.3	39.8	62.1	14.1	115.631	< 0.001*
[b]Ce ppm	1	0	22.9	32	16	56.1	70	27	37	70	20	37	63	14	115.409	< 0.001*
[ab]Sn ppm	0.1	0	0.9	2.1	0.4	1.9	2.5	1.0	1.6	17.3	0.6	1.2	2.3	0.4	102.728	< 0.001*
[b]Y ppm	0.1	0	5.8	9.7	3.3	14.7	24.1	6.9	9.7	18.1	4.0	10.0	18.1	2.6	112.848	< 0.001*
[ab]Nb ppm	0.1	0	3.9	6.8	2.5	8.7	10.5	4.4	6.0	9.9	2.4	5.4	9.4	1.1	111.839	< 0.001*
Ta ppm	0.1	0	0.2	0.6	0.1	0.6	0.8	0.3	0.4	0.8	0.1	0.4	0.7	0.1	115.228	< 0.001*
Be ppm	1	14.7	1	2	1	2	3	1	2	2	1	1	2	1	6.050	0.014
Sc ppm	1	0	3	4	1	8	11	3	5	11	1	5	9	1	118.358	< 0.001*
Li ppm	0.1	0	9.5	12.0	7.2	24.9	34.2	11.9	16.3	31.5	8.1	17.8	28.2	7.3	116.105	< 0.001*
S%	0.1	100	–	–	–	–	–	–	–	–	–	–	–	–		
Rb[cd] ppm	0.1	0	74.1	82.7	83.8	61.6	100.0	59.9	79.3	100	61.7	86.0	91.3	78.1	15.693	< 0.001*
Hf ppm	0.1	0	0.7	1.0	0.4	1.9	2.6	0.9	1.3	2.2	0.7	1.2	1.9	0.4	117.158	< 0.001*
In ppm	0.05	85.3	–	–	–	0.06	0.08	0.05	0.06	0.07	0.05	0.05	0.05	< 0.05		
Re ppm	0.005	99.4	–	–	–	–	–	–	–	–	–	–	–	–		
Se ppm	1	98.1	–	–	–	–	–	–	–	–	–	–	–	–		
Te[d] ppm	0.5	92.9	–	–	–	0.7	1.0	0.5	0.7	0.9	0.5	–	–	–		
[b]Tl ppm	0.5	55.8	0.5	0.6	0.5	0.5	0.6	0.5	0.5	0.6	0.5	0.5	0.6	< 0.5	0.019	0.925
χ_{lf}[d] $10^{-8}\,m^3\,kg^{-1}$	0.1	0	18.4	41.2	1.8	38.4	68.5	19.0	28.8	68.5	5.7	15.0	28.2	2.0	84.977	< 0.001*
[b]χ_{hf} $10^{-8}\,m^3\,kg^{-1}$	0.1	0	18.1	41.3	3.6	37.4	63.7	18.2	28.5	63.7	5.4	14.9	28.9	3.6	90.184	< 0.001*

(*continued on next page*)

Table 2 (*continued*)

Element	MDL	Elements < MDL in source samples (%)	Value in source samples						Value in sediment samples						*H* value	*P* value
			Sand from Mu Us Sandy Land			Loess from loess hills			Sheet sand hills			Soil profile				
			Mean	Max.	Min.	Mean	Max.	Min.	Mean	Max.	Min.	Mean	Max.	Min.		
[b]M_z-1 Φ	0.01	0	2.04	3.88	1.60	5.14	6.12	4.34	3.52	5.79	1.74	2.83	4.88	0.94	116.236	< 0.001*
M_z-2 Φ	0.01	0										3.36	4.88	1.81	116.236	< 0.001*

MDL refers to minimum detectable level; M_z refers to mean grain size, M_z-1 represents the data for all 33 samples collected in the 320 cm depth soil profile, while M_z-2 represents the 24 soil samples with the exception of nine samples in the 210 and 290 cm soil profile layer.

[a] The concentration range of these elements in sediment samples (sand sheet hills) were outside the range of their source values.

[b] The concentration range of these elements in sediment samples (soil profiles) were outside the range of their source values.

[c] The mean concentration range of these elements in sediment samples (sand sheet hills) were outside the range of their source category mean values.

[d] The mean concentration range of these elements in sediment samples (soil profiles) were outside the range of their source category mean values.

* The significance level was a = 0.05. χ_{lf} and χ_{hf} refer to low-and high-frequency magnetic susceptibility, respectively.

sediment came from both local loess and sand from the Mu Us Sandy Land. Grain size is an important factor used for the description of sediment characteristics based on both artificial mixture tests and discriminant sediment sources (Tables 1 and 3). Sediment source contribution estimation results based on grain size classification indicated that loess were primarily from local area (90.5% ± 0.5%), sand sheets on loess hills were primarily from the Mu Us Sandy Land (95.0% ± 0.5%), while greater than half of the mixtures were from the sandy land area (61.1% ± 0.1%) (Table 4). Moreover, the contributions of sand from the Mu Us Sandy Land and loess from local slopes to sand sheet sediment deposits on hills roughly fitted logarithmic functions ($R^2 = 0.85$). To simplify the classification of grain size for sand sheet distribution on hills, particles coarser than 3.32 Φ (> 100 μm) came primarily from the Mu Us Sandy Land, while finer particles came from local loess slopes as a whole (Fig. 5). This indicated that the particle grain size was a key factor to divide the sediment source in the sand sheet area. Wind erosion dominated the transport of sand from the Mu Us Sandy Land to the hilly loess area. These results also confirmed that the multiple composite fingerprinting technique is feasible for the study of sediment sources in the wind-water erosion crisscross region on the CLP.

3.4. Source discrimination of sand in the soil profile

For depth incremental samples collected in the soil profile, the constraint conditions removed undetectable elements, including Ag, Cd, Bi, S, In, Re, Se, Te, and Tl, namely, element whose concentration range in the sediment samples were beyond the range of their source values (Mo, Cu, Pb, Ni, Co, Mn, Fe, U, Th, V, Ca, P, Cr, Mg, Al, Zr, Ce, Sn, Y, Nb, χ_{hf}, and M_z) and elements whose mean concentration in sediment were outside source category means (Rb and χ_{lf}). The Kruskal-Wallis *H* test screened out a non-significant factor (Be) (Table 2). The remaining 14 factors differed significantly among the potential sources, and they subsequently underwent stepwise DFA and variability analysis. Finally, five factors were comprised of the optimum composite fingerprints, including Zn, Ti, As, Sr, and Li. These optimum composite fingerprinting factors correctly classified sediment sources with a cumulative correct classification of 94.9% (Table 5). In the soil profile, even though the sediment contribution estimation using the multivariate mixing model indicated that very coarse sediment (with a mean grain size of 1.43 Φ) collected from nine depth intervals in the 210 and 290 cm soil profile came from the Mu Us Sandy Land, these samples had very low GOF (an average of 24.7%). This meant that the sediment contribution results were unacceptable, that is to say, there was high possibility that sediment in the 210 and 290 cm soil profile was from other unknown sources rather than sand from the Mu Us Sandy Land and local loess. Thus, we removed these nine depth intervals, and found that grain size was included into the optimum composite multiple fingerprinting factors. The final optimum composite multiple fingerprinting factors were Zn, Ti, As, Sr, Li, and M_z, which were further confirmed by correspondence analysis (Fig. 6), having correctly classified sediment sources with a cumulative correct classification of 100% (Table 6).

3.5. Source apportionment of sand in the soil profile

For the 24 samples collected in the soil profile, GOF ranged from 71.6% to 92.6% and averaged 81.9%. The sediment contribution from the Mu Us Sandy Land was 50.3% ± 0.4%, while it was 49.7% ± 0.4% from local loess. Similar to sand sheets on loess hills, sediment sources varied significantly between sampling layers. The sediment contribution of certain sites came entirely from local loess, while that of other sites came entirely from the Mu Us Sandy Land. For the remaining sites, sediment contribution came from both local loess and the Mu Us Sandy Land. For loess, sand and mixture classified based on grain size, loess was primarily from the local loess area

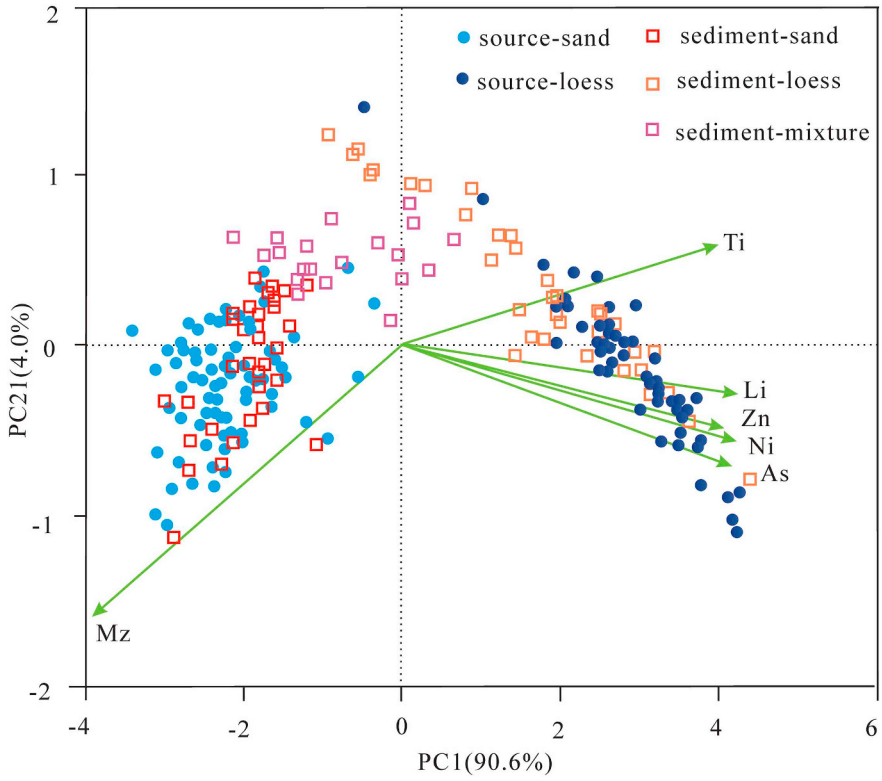

Fig. 4. Correspondence analysis produced using biplots between source and sediment samples collected on the sampling transect.

Table 3
Optimal fingerprinting properties based on discrimination results of sand-loess hills.

Step	Selected fingerprinting property	Cumulative correct classification of the source (%)	Correct classification of the source based on a single fingerprinting property (%)
1	Zn	92.9	91.7
2	Ti	94.2	93.6
3	As	94.2	93.6
4	Ni	94.2	94.9
5	Li	94.9	94.9
6	M_z	100	99.4

Table 4
The contribution of sand and loess to sediment in the sand sheet area based on grain size classification.

Soil type of sand sheet slopes	Mean grain size of sediment (Φ)	Contribution (%)	
		Local loess	Sand from Mu Us Sandy Land
Loess	4.43	90.5 ± 0.5	9.5 ± 0.5
Mixture	2.79	38.9 ± 0.1	61.1 ± 0.1
Sand	1.99	5.0 ± 0.5	95.0 ± 0.5

(88.8% ± 0.5%), while sand was primarily from the Mu Us Sandy Land (93.1% ± 0.6%), and greater than half of the mixtures were from local loess hills (55.0% ± 0.1%) and less than half from the sandy land (45.0% ± 0.1%) (Table 7). This phenomenon revealed the considerable variation in historical sediment sources, and demonstrated the climate change effects in the study region.

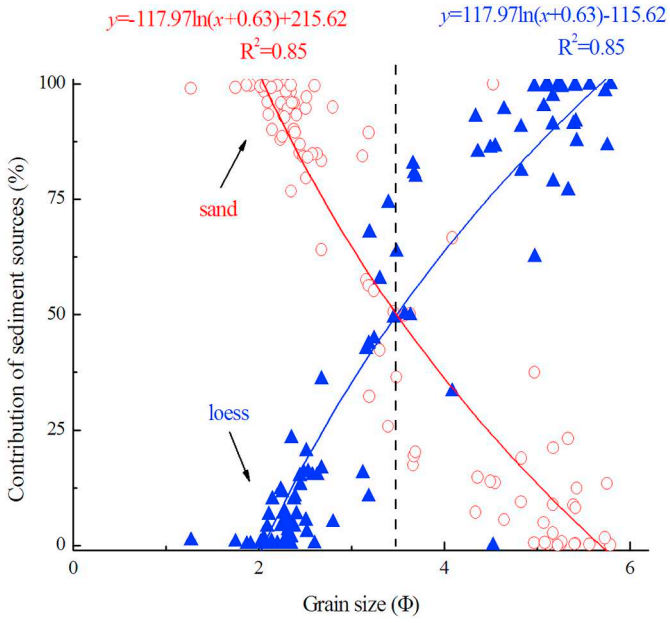

Fig. 5. The contribution of particles in different grain size to sediments on sand-loess hills.

4. Discussion

4.1. Aeolian effect on sand deposition

Because sand sheet deposits on loess hills were aligned in a northwest to southeast direction in this study, sand was observed from the toe to the top of hills on both aspects. However, the inclination of sand deposition was on leeward slopes and the flat areas of hills. The contribution of sand to sediment on windward slopes averaged

Table 5
Optimal fingerprinting properties based on discrimination results for sediment in the whole soil profile (33 samples).

Step	Selected fingerprinting property	Cumulative correct classification of the source (%)	Correct classification of the source based on a single fingerprinting property (%)
1	Zn	91.7	91.7
2	Ti	94.2	93.6
3	As	94.2	93.6
4	Sr	94.9	94.9
5	Li	94.9	94.9

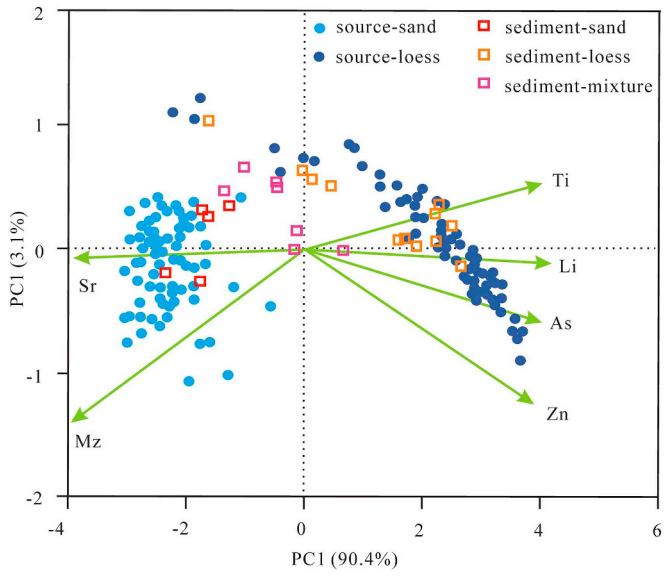

Fig. 6. Correspondence analysis produced using biplots between source and sediment samples collected in the soil profile.

Table 6
Optimal fingerprinting properties based on discrimination results for sediment in the soil profile with the exception of nine samples in the 210 and 290 cm soil profile layer (24 samples).

Step	Selected fingerprinting property	Cumulative correct classification of the source (%)	Correct classification of the source based on a single fingerprinting property (%)
1	Zn	91.7	91.7
2	Ti	94.2	93.6
3	As	94.2	93.6
4	Sr	94.9	94.9
5	Li	94.9	94.9
6	M_z	100	99.4

Table 7
Contribution of sand and loess to sediment in the soil profile based on grain size classification.

Soil type in the profile layers	Number of layers	Mean grain size of sediment (Φ)	Contribution (%)	
			Local loess	Sand from Mu Us Sandy Land
Loess	6	3.91	88.8 ± 0.5	11.2 ± 0.5
Mixture	12	2.84	55.0 ± 0.1	45.0 ± 0.1
[a]Sand	6	2.00	6.9 ± 0.6	93.1 ± 0.6

[a] Nine samples from 210 to 290 cm in the soil profile layer were removed from the contribution analysis due to their low GOF.

33.3% ± 0.4%, while it averaged 67.3% ± 0.4% on leeward slopes. Because the local prevailing wind is from the northwest, eroded particles, especially coarse particles transported from the northwestern area, were more likely to be deposited on slopes subject to relatively light wind energy, including leeward slopes, flat areas and concave areas sheltered from the wind (Fig. 7). For convex landforms, winds often accelerate from windward slopes to the top of hills (Bo and Zheng, 2013). Thus, erosion (not deposition) occurred in these areas, which did not result in the settling of sand (deposition). This implied that aeolian activity significantly affected the distribution of sand on loess hills. The strong winter monsoon drove loose sand particles from the Mu Us Sandy Land, moving them in a southeast direction. The transported particles finally deposited in the hilly area (Stevens et al., 2013).

4.2. The combined effect of wind and water erosion on sediment redistribution

A slope-scale study conducted by Zhang et al. (2018) in this region using cesium-137 (Cs-137) measurements suggested that the contribution of wind erosion was roughly 30% on windward (northern and northwestern) slopes, which attested to the significant effects of water erosion in the study region. Given the importance of water erosion processes, the distribution of sand sheets was the result of the combined effect of wind and water erosion. However, Zhang et al. (2018) conducted their study on a loess slope devoid of sand, and the effect of wind and water to soil redistribution on sand sheet hills should consequently differ from results of this study. The impact of wind erosion on sand sheet slopes was more comparable to loess slopes when taking into account the sorting variation of particles. Sorting coefficients for loess covered sampling sites (with an average of 2.19 Φ ± 0.18 Φ) were worse than for sand sites (with an average of 1.31 Φ ± 0.43 Φ) on sand sheet hills, and the sorting coefficient of mixture distributed areas were between that of sand and loess areas (with an average of 1.83 Φ ± 0.48 Φ). By comparing two opposite slopes with sand sheet deposits, results of mean sorting coefficients from northwestern aspects were 2.27 ± 0.26 Φ, 1.95 ± 0.32 Φ, and 1.57 ± 0.45 Φ for the three sampled slopes, respectively, while results were 2.01 ± 0.46 Φ, 1.52 ± 0.50 Φ, and 1.46 ± 0.67 Φ on southeastern aspects, respectively (Fig. 8). Better sorting on leeward slopes further revealed the combined effect of wind and water erosion, given that the sorting effect of wind is typically stronger than water when particles are transported the same distance (Skidmore and Powers, 1982). The stronger sorting capacity of wind will result in better sorting of particles, and erosion processes driven by multiple agencies in the same direction (southeastern slope) will improve sorting compared to the opposite direction (northwestern slope).

4.3. Environmental changes in the wind-water erosion crisscross region as indicated by sediment deposition

The obvious grain size variation in the soil profile taken from a specific sand sheet hill (LS2) clearly showed the stratified distribution of sand and loess, which indicated the environmental change in the transition region and how it affected sediment sources. The variation tendency was similar between grain size, sorting coefficients (expressed by the SD of grain size), and the contribution of sediment sources from loess hills (Fig. 9). Variation in sediment deposition in the soil profile could provide evidence for environmental changes, based on grain size variation, particle sorting, and sediment source contribution. Following the deposition sequence, we found that the 320 cm soil profile suddenly changed from loess to sand, and then loess gradually replaced sand at an approximate depth of 210 cm, after which sand deposited above the loess sediment again. This profile could be classified into five comprehensive stages. In stages 1 and 4, sediment was mainly composed of local loess, for which the contribution of loess to sediment averaged 96.0% ± 0.9% and 70.3% ± 0.2%, respectively. This indicated that

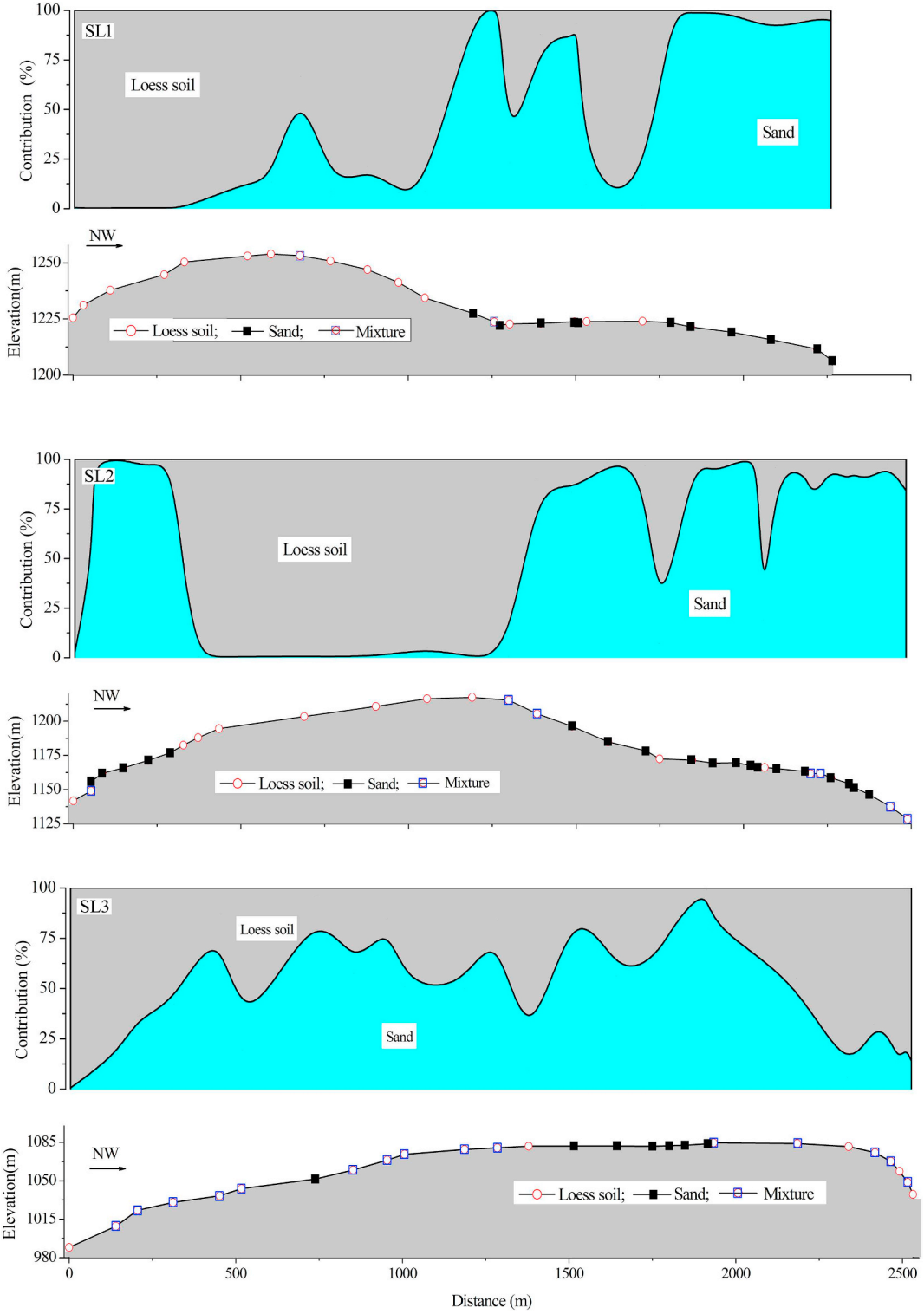

Fig. 7. Distribution of sediment source contributions on studied hills.

during these particular sedimentation periods, the influence of the Mu Us Sandy Land on sand sheet deposition in hilly areas was very limited, which means that aeolian activity was relatively weak. However, we found that a layer in stage 4 had a higher sediment contribution from the Mu Us Sandy Land. Sediment particles became progressively finer from stage 2 to the deeper layers of stage 4. This implied that changing environmental conditions continued throughout this period, and the Mu Us Sandy Land as a source to adjacent loess hills continuously decreased. In stage 2, sediment was coarser than potential source sediments selected for this study, and these sources have not been established. This demonstrated that there must have been other sediment sources in this crisscross region. In stage 5, sediment was primary sand (with an average of 69.6% ± 0.2%) (Fig. 9a). This means that aeolian activities were strong during this period, and sand was transported from the Mu Us Sandy Land in a southeastern direction. Overall, the soil profile recorded spatial variation on the edge of the Mu Us Sandy Land. Deposited sediment alternated between local loess and sand from the Mu Us Sandy Land.

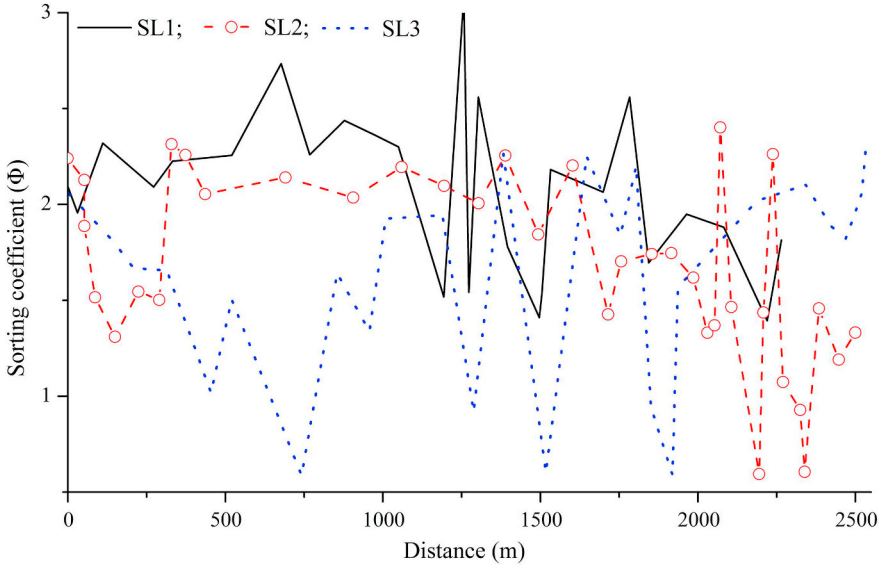

Fig. 8. Variation in the sorting coefficient on sand sheet hills along sampling transects (the sorting coefficient was represented by the standard deviation of grain size using the formula by Folk and Ward (1957)).

The 320 cm sediment deposition layer was formed at approximately 12.85 ka BP, and the formation of the top 10 cm soil layer took 2.64 ka BP, as indicated by radiocarbon dating (Table 8). Anthropogenic activities started to strongly affect the environmental evolution at 2.0 ka BP in the study region (Ma, 2011). Although manmade fires accelerated the desertification of the region starting at approximately 4.6 ka BP, such fires mainly contributed to desertification, rather than to the movement of sand boundaries (Miao et al., 2016). Thus, the movement of the Mu Us Sandy Land edge was primarily caused by climate change. Previous studies on the relationships between sediments and climatic changes conducted in the Mu Us Sandy Land and the transition zone between the Mu Us Sandy Land and the Loess Plateau, have indicated that the fluctuation between dry and wet climate change conditions during the Holocene played a role in the sensitivity of these ecosystems (Jia et al., 2015; Liu et al., 2014; B. Liu et al., 2016; B.L. Liu et al., 2016; Ma, 2011). This phenomenon is also reflected in the soil profile used in this study. The representative proxy indicators used in a study by Liu et al. (2014), including Rb/Sr and the chemical index of alteration (CIA) (CIA = $[Al_2O_3/(Al_2O_3 + CaO + K_2O + Na_2O)] \times 100\%$), also revealed conditions of climate change. Values of Rb/Sr reflected changes in moisture, while CIA reflected sediment weathering. The variation tendency of Rb/Sr and the CIA was coincided in this study. High values of Rb/Sr and the CIA indicated the influence of strong East Asian summer monsoons and an increase in precipitation, while low values of Rb/Sr and

Table 8
Radiocarbon (^{14}C) dating analysis of four sediment layers.

Collection depth of sample (cm)	Measured radiocarbon age (ka BP)	[a]Conventional radiocarbon age (ka BP)
0–10	2.61 ± 0.03	2.64 ± 0.03
70–80	8.94 ± 0.03	9.01 ± 0.03
130–140	12.79 ± 0.04	12.85 ± 0.04
320–330	11.14 ± 0.03	11.19 ± 0.03

[a] Corrected based on ^{13}C results.

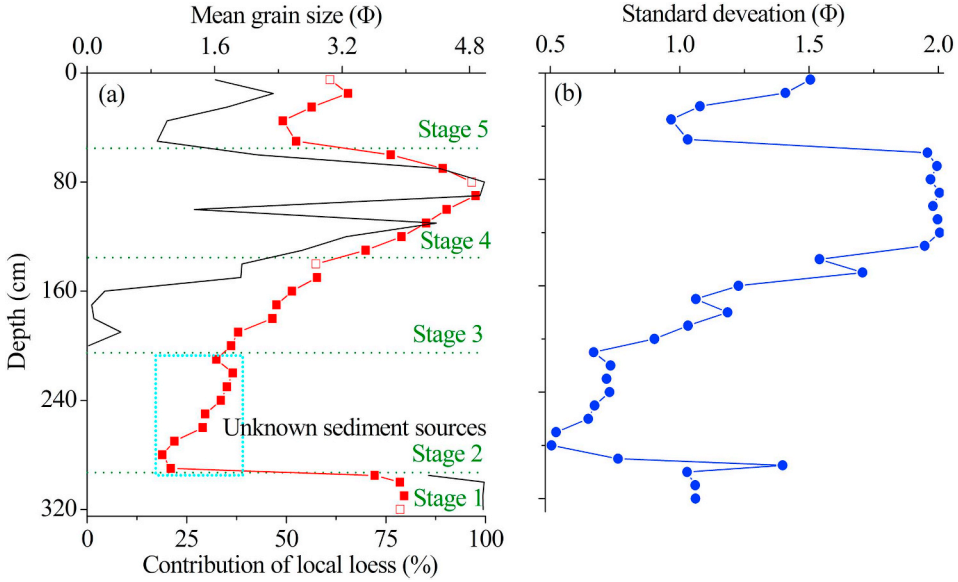

Fig. 9. Variation in grain size (a), sorting coefficient (b) (expressed as the standard deviation of the grain size) of sediment particles, and the contribution of loess to sediment in the soil profile (a) (the empty square represents analyzed dating samples using radiocarbon data (^{14}C)).

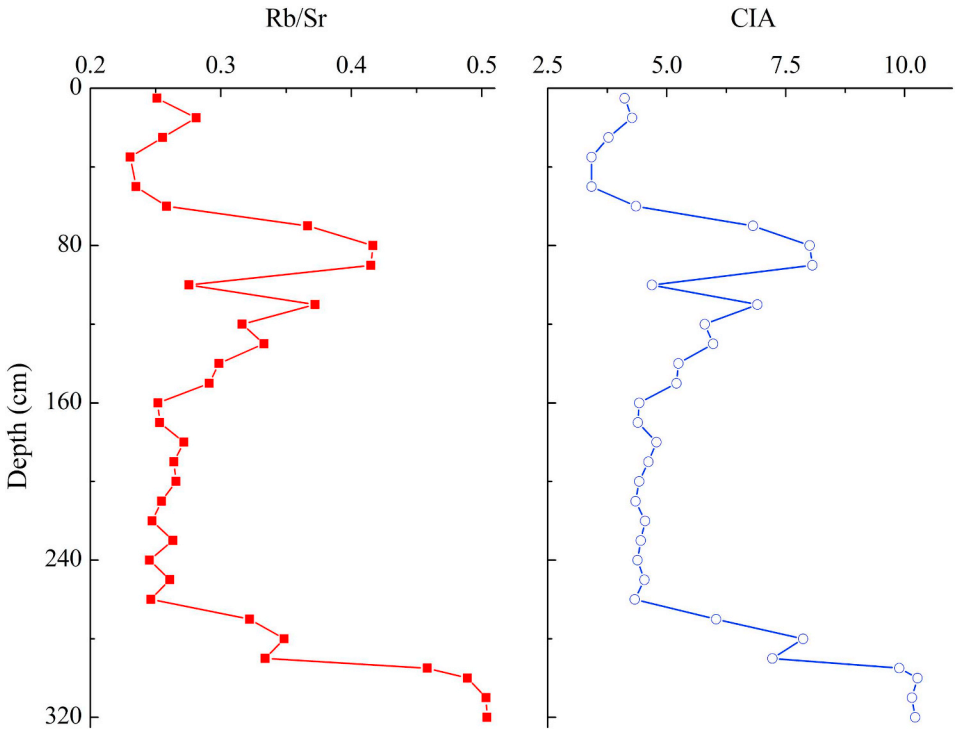

Fig. 10. Variation in Rb/Sr and the chemical index of alteration (CIA) in the soil profile.

the CIA indicated a drier climate under weak summer monsoonal conditions (Fig. 10). Thus, it is obvious that most of the study region was dominated by a dry climate at approximately 12.85 ka BP. This finding is consistent with previous studies (Jia et al., 2015; B. Liu et al., 2016; B.L. Liu et al., 2016; Wang et al., 2001).

4.4. Study limitations

Sand sheets were discretely distributed on loess hills, and loess was exposed on slopes in some areas. Given erosive winds that transport aeolian sand south have different energy levels, even though the formation of sand distribution on loess hills occurred during a particular period in this region, it could not have occurred during a single erosion event. We were unable to determine the reasons behind sand movement transported over certain hilly areas, and formed areas covered by loess only. Additionally, we are also unable to clarify the environmental conditions that prevented aeolian sand from settling and forming sand sheets. Although results of this study indicated the combined effect of wind and water erosion on sediment redistribution, it failed to quantitatively distinguish between the influence of wind and water erosion on the redistribution of sand when transported to hilly areas. It is unknown how the complicated processes of wind and water erosion affect the redistribution and transport of sediment, and what the amount of sediment has transported to downstream rivers. Thus, we are far from understanding the effect of wind and water erosion on the redistribution of sediment. Although we reestablished historical climate change from sediment deposition in a soil profile in the study region, we have not yet been able to determine the scope of sand transport from the Mu Us Sandy Land to the loess hills during each stage, and have also not yet determined the source of the very course sediment (stage 2). In order to solve these issues, it is essential to expand study scales both spatially and temporally to get a better understanding of local historical climate change and variation of environmental conditions.

The representativeness of samples is important for sediment tracing. We carefully selected the sampling transect and deposition profile while taking into account factors such as soil type, landform, vegetation, and land use. However, the study area is limited considering the scope of sediment transportation, and sediment transport was complicated caused by multiple local erosion agencies. Thus, it is also necessary to expand study scales both spatially and temporally to obtain samples that are more representative. Additionally, the sediment tracing procedure adopted in this study could cause to the result uncertainties. We did not consider the correction of particle size and organic matter when we selected the model because recent studies have suggested that they were non-conservative properties having a negative effect on sediment source discrimination (Collins et al., 2017; Laceby and Olley, 2015; Pulley et al., 2017). In order to obtain robust optimal fingerprinting factors, rigorous statistical tests should be applied in the selection process to decrease the uncertainty of sediment source discrimination. This is because simple statistical tests could allow some properties to pass screening, and be group together with optimal fingerprinting factors, increasing the error of the mixing model.

5. Conclusions

This study provides valuable information on sand sheet sources in the wind-water erosion crisscross region of the CLP using the composite fingerprinting approach. Optimal composite fingerprinting factors correctly classified the sediment sources on sand sheet hills at 100%, and also correctly classified sediment sources in a 320 cm soil profile at 100% with the exception of very coarse sediment from 210 to 290 cm in the soil profile. Results demonstrated that at least half of all sediment on sand-loess hills, was from the sandy land areas with significant observed spatial variation. Sand coarser than 100 μm was primarily transported from the Mu Us Sandy Land, while finer particles were primarily transported from loess hills. Wind played a key role in the transport of sand from the Mu Us Sandy Land to the loess hill area, and the combined effect of wind and water erosion contributed significantly to the redistribution of sand, which has led to the current distribution pattern of sand in the study area. Variation in deposits in the soil profile reflects the environmental changes, especially aeolian activities, which were primarily attributed to climate change. This study analyzed sand sources in the wind-water erosion crisscross region on the CLP, and attests to the feasibility of the multiple composite fingerprinting

approach for sediment source studies. However, owing to the fact that the landforms, soils, and land use types added to the complexity of erosion processes, it will be necessary to expand study scales to better understand sediment transport processes in this region.

Acknowledgements

This study was financially supported by the National Natural Science Foundation of China (41671281, 41561144011, and 41761144060), the Special Fund for Basic Scientific Research of the Northwest A & F University of the Ministry of Education (2452015095), and the Special Funds of Scientific Research Programs of the State Key Laboratory of Soil Erosion and Dryland Farming on the Chinese Loess Plateau of the Ministry of Science and Technology (A314021403-C2). The authors sincerely appreciate the editor and two anonymous reviewers for their valuable comments.

References

Bo, T.L., Zheng, X.J., 2013. Wind speed-up process on the windward slope of dunes in dune fields. Comput. Fluids 71, 400–405.
Bullard, J.E., Livingstone, I., 2002. Interactions between aeolian and fluvial systems in dryland environments. Area 34 (1), 8–16.
Chen, F.X., Fang, N.F., Wang, Y.X., Tong, L.S., Shi, Z.H., 2017. Biomarkers in sedimentary sequences: indicators to track sediment sources over decadal timescales. Geomorphology 278, 1–11.
Collins, A.L., Walling, D.E., 2002. Selecting fingerprint properties for discriminating potential suspended sediment sources in river basins. J. Hydrol. 261, 218–244.
Collins, A.L., Walling, D.E., 2004. Documenting catchment suspended sediment sources: problems, approaches and prospects. Progr. Phys. Geogr. 28 (2), 159–196.
Collins, A.L., Walling, D.E., Leeks, G.J.L., 1997. Source type ascription for fluvial suspended sediment based on a quantitative composite fingerprinting technique. Catena 29, 1–27.
Collins, A.L., Zhang, Y., Walling, D.E., Grenfell, S.E., Smith, P., 2010. Tracing sediment loss from eroding farm tracks using a geochemical fingerprinting procedure combining local and genetic algorithm optimization. Sci. Total Environ. 408 (22), 5461–5471.
Collins, A.L., Pulley, S., Foster, I.D.L., Gellis, A., Porto, P., Horowitz, A.J., 2017. Sediment source fingerprinting as an aid to catchment management: a review of the current state of knowledge and a methodological decision-tree for end-users. J. Environ. Manag. 194, 86–108.
Field, J.P., Breshears, D.D., Whicker, J.J., 2009. Toward a more holistic perspective of soil erosion: why aeolian research needs to explicitly consider fluvial processes and interactions. Aeolian Res. 1, 9–17.
Folk, R.L., Ward, W.C., 1957. Brazos River bar, a study in the significance of grain-size parameters. J. Sediment. Petrol. 27, 3–26.
Gellis, A.C., Walling, D.E., 2013. Sediment source fingerprinting (tracing) and sediment budgets as tools in targeting river and watershed restoration programs. In: Simon, A., Bennett, S.J., Castro, J.M. (Eds.), Stream Restoration in Dynamic Fluvial Systems: Scientific Approaches, Analyses, and Tools. Geophysical Monograph Series: Washington, vol. 194. pp. 263–291. https://doi.org/10.1029/2010GM000960.
Gholami, H., Telfer, M.W., Blake, W.H., Fathabadi, A., 2017. Aeolian sediment fingerprinting using a Bayesian mixing model. Earth Surf. Process. Landforms 42 (14), 2365–2376.
Grousset, F.E., Biscaye, P.E., 2005. Tracing dust sources and transport patterns using Sr, Nd and Pb isotopes. Chem. Geol. 222, 149–167.
Guerra, A.J.T., Fullen, M.A., Jorge, M.C.O., Bezerra, J.F.R., Shokr, M.S., 2017. Slope processes, mass movement and soil erosion: a review. Pedosphere 27 (1), 27–41.
Haddadchi, A., Ryder, D.S., Evrard, O., Olley, J., 2013. Sediment fingerprinting in fluvial systems: review of tracers, sediment sources and mixing models. Int. J. Sediment Res. 28 (4), 560–578.
Haddadchi, A., Olley, J., Laceby, P., 2014. Accuracy of mixing models in predicting sediment source contributions. Sci. Total Environ. 497-498, 139–152.
Hu, F.G., Yang, X.P., 2016. Geochemical and geomorphological evidence for the provenance of aeolian deposits in the Badain Jaran Desert, northwestern China. Quat. Sci. Rev. 131 (A), 179–192.
Jia, X.P., Wang, H.B., Xiao, J.H., 2011. Geochemical elements characteristics and sources of the riverbed sediment in the yellow river's desert channel. Environ. Earth Sci. 64, 2159–2173.
Jia, F.F., Lu, R.J., Gao, S.Y., Li, J.F., Liu, X.K., 2015. Holocene aeolian activities in the southeastern Mu Us Desert, China. Aeolian Res. 19, 267–274.
Koiter, A.J., Owens, P.N., Petticrew, E.L., Lobb, D.A., 2013. The behavioural characteristics of sediment properties and their implications for sediment fingerprinting as an approach for identifying sediment sources in river basins. Earth-Sci. Rev. 125, 24–42.
de la Paix, M.J., Lanhai, L., Xi, C., Varenyam, A., Nyongesah, M.J., Habiyaremye, G., 2013. Physicochemical properties of saline soils and aeolian dust. Land Degrad. Dev. 24 (6), 539–547.
Laceby, J.P., Olley, J., 2015. An examination of geochemical modelling approaches to tracing sediment sources incorporating distribution mixing and elemental correlations. Hydrol. Process. 29 (6), 1669–1685.
Lamba, J., Karthikeyan, K.G., Thompson, A.M., 2015. Apportionment of suspended sediment sources in an agricultural watershed using sediment fingerprinting. Geoderma 239–240, 25–33.
Liang, L.J., Sun, Y.B., Beets, C.J., Prins, M.A., Wu, F., Vandenberghe, J., 2013. Impacts of grain size sorting and chemical weathering on the geochemistry of Jingyuan loess in the northwestern Chinese Loess Plateau. J. Asian Earth Sci. 69, 177–184.
Liang, M.Y., Wang, Z.X., Zhou, S., Zong, K.Q., Hu, Z.C., 2014. The provenance of Gansu Group in Longxi region and implications for tectonics and paleoclimate. Sci. China Earth Sci. 57 (6), 1221–1228.
Liu, B., Jin, H.L., Sun, L.Y., Sun, Z., Niu, Q.H., Xie, S.B., Li, G.H., 2014. Holocene moisture change revealed by the Rb/Sr ratio of aeolian deposits in the southeastern Mu Us Desert, China. Aeolian Res. 13, 109–119.
Liu, B., Jin, H.L., Sun, Z., Zhao, S., 2016. Geochemical weathering of aeolian sand and its palaeoclimatic implications in the Mu Us Desert, northern China, since the Late Holocene. J. Arid Land 8 (5), 647–659.
Liu, B.L., Niu, Q.H., Qu, J.J., Zu, R.P., 2016. Quantifying the provenance of aeolian sediments using multiple composite fingerprints. Aeolian Res. 22, 117–122.
Ma, J., 2011. OSL Dating Holocene Sequence and Palaeoclimate Change Records in Southern Margin of Mu Us Desert, North China. Northwest University, Xi'an (in Chinese).
Manjoro, M., Rowntree, K., Kakembo, V., Foster, I., Collins, A.L., 2017. Use of sediment source fingerprinting to assess the role of subsurface erosion in the supply of fine sediment in a degraded catchment in the Eastern Cape, South Africa. J. Environ. Manag. 194, 27–41.
McKinley, R., Radcliffe, D., Mukundan, R., 2013. A streamlined approach for sediment source fingerprinting in a Southern Piedmont watershed, USA. J. Soils Sediments 13 (10), 1754–1769.
Miao, Y.F., Jin, H.L., Cui, J.X., 2016. Human activity accelerating the rapid desertification of the Mu Us Sandy Lands, North China. Sci. Rep. 6, 23003. https://doi.org/10.1038/srep23003.
Müller-Nedebock, D., Chaplot, V., 2015. Soil carbon losses by sheet erosion: a potentially critical contribution to the global carbon cycle. Earth Surf. Process. Landforms 40, 1803–1813.
Nie, J.S., Stevens, T., Rittner, M., Stockli, D., Garzanti, E., Limonta, M., Bird, A., Ando, S., Vermeesch, P., Saylor, J., Lu, H.Y., Breecker, D., Hu, X.F., Liu, S.P., Resentini, A., Vezzoli, G., Peng, W.B., Carter, A., Ji, S.C., Pan, B.T., 2015. Loess Plateau storage of Northeastern Tibetan Plateau-derived Yellow River sediment. Nat. Commun. 6, 8511. https://doi.org/10.1038/ncomms9511.
Osterkamp, W.R., Hupp, C.R., Stoffel, M., 2012. The interactions between vegetation and erosion: new directions for research at the interface of ecology and geomorphology. Earth Surf. Process. Landforms 37, 23–36.
Palazón, L., Latorre, B., Gaspar, L., Blake, W.H., Smith, H.G., Navas, A., 2015. Comparing catchment sediment fingerprinting procedures using an auto-evaluation approach with virtual sample mixtures. Sci. Total Environ. 532, 456–466.
Pimentel, D., 2006. Soil erosion: a food and environmental threat. Environ. Dev. Sustain. 8 (1), 119–137.
Pulley, S., Foster, I., Collins, A.L., 2017. The impact of catchment source group classification on the accuracy of sediment fingerprinting outputs. J. Environ. Manag. 194, 16–26.
Rowntree, K.M., van der Waal, B.W., Pulley, S., 2017. Magnetic susceptibility as a simple tracer for fluvial sediment source ascription during storm events. J. Environ. Manag. 194, 54–62.
Sherriff, S.C., Franks, S.W., Rowan, J.S., Fenton, O., Uallachain, D.O., 2015. Uncertainty-based assessment of tracer selection, tracer non-conservativeness and multiple solutions in sediment fingerprinting using synthetic and field data. J. Soils Sediments 15, 2101–2116.
Skidmore, E.L., Powers, D.H., 1982. Soil aggregate stability energy-based index. Soil Sci. Soc. Am. J. 46, 1274–1279.
Stevens, T., Carter, A., Watson, T.P., Vermeesch, P., Andò, S., Bird, A.F., Lu, H., Garzanti, E., Cottam, M.A., Sevastjanova, I., 2013. Genetic linkage between the Yellow River, the Mu Us desert and the Chinese Loess Plateau. Quat. Sci. Rev. 78, 355–368.
Tang, K.L., Hou, Q.C., Wang, B.K., Zhang, P.C., 1993. The environment background and administration way of wind-water erosion crisscross region and Shenmu experimental area on the loess plateau. In: Memoir of Northwest Institute of Soil and Water Conservation, Academia Sinica and Ministry of Water Resources. 18. pp. 1–15 (in Chinese).
Torfstein, A., Teutsch, N., Tirosh, O., Shaked, Y., Rivlin, T., Zipori, A., Stein, M., Lazar, B., Erel, Y., 2017. Chemical characterization of atmospheric dust from a weekly time series in the north Red Sea between 2006 and 2010. Geochim. Cosmochim. Acta 211, 373–393.
USDA, 1951. United Sates Department of Agriculture (USDA) Soil Survey Manual. US. Department of Agriculture Handbook No. 18 (1951). (Washington, DC).
Walling, D.S., 2013. The evolution of sediment source fingerprinting investigations in fluvial systems. J Soils Sediment. 13 (10), 1658–1675.
Walling, D.E., Owens, P.N., Leeks, G.J.L., 1999. Fingerprinting suspended sediment sources in the catchment of the River Ouse, Yorkshire, UK. Hydrol. Proc. 13 (7), 955–975.
Wang, Y.J., Cheng, H., Edwards, R.L., An, Z.S., Wu, J.Y., Shen, C.C., Dorale, J.A., 2001. A high-resolution absolute-dated late pleistocene monsoon record from Hulu cave, China. Science 294, 2345–2348.
Wang, X.M., Lang, L.L., Li, H., Hua, T., Wang, G.T., Zhou, N., 2015. Geochemical evidence for seasonal variations in potential loess sources of the western Chinese Loess Plateau. Atmos. Environ. 120, 369–375.
Wang, S., Fu, B.J., Piao, S.L., Lü, Y.H., Ciais, P., Feng, X.M., Wang, Y.F., 2016. Reduced sediment transport in the Yellow River due to anthropogenic changes. Nat. Geosci. 9, 38–41.

Wang, Z.X., Liang, M.Y., Sun, Y.Q., Dai, G.W., 2017. Cenozoic tectonic and geomorphic evolution of the Longxi region in northeastern Tibetan Plateau interpreted from detrital zircon. Sci. China Earth Sci. 60 (2), 256–267.
Weltje, G.J., 2012. Quantitative models of sediment generation and provenance: state of the art and future developments. Sediment. Geol. 280, 4–20.
Wilkinson, S.N., Hancock, G.J., Bartley, R., Hawdon, A.A., Keen, R.J., 2013. Using sediment tracing to assess processes and spatial patterns of erosion in grazed rangelands, Burdekin River basin, Australia. Agric. Ecosyst. Environ. 180, 90–102.
Williams, M., 2015. Interactions between fluvial and aeolian geomorphic systems and processes: examples from the Sahara and Australia. Catena 134, 4–13.
Yang, X.P., Zhu, B.Q., White, P.D., 2007. Provenance of aeolian sediment in the Taklamakan Desert of western China, inferred from REE and major-elemental data. Quat. Int. 175, 71–85.
Yu, K.F., Hartmann, K., Nottebaum, V., Stauch, G., Lu, H.Y., Zeeden, C., Yi, S.W., Wünnemann, B., Lehmkuhl, F., 2016. Discriminating sediment archives and sedimentary processes in the arid endorheic Ejina Basin, NW China using a robust geochemical approach. J. Asian Earth Sci. 119, 128–144.
Zhang, X.C., Liu, B.L., 2016. Using multiple composite fingerprints to quantify fine sediment source contributions: a new direction. Geoderma 268, 108–118.
Zhang, F.B., Bai, Y.J., Xie, L.Y., Yang, M.Y., Li, Z.B., Wu, X.R., 2017. Runoff and soil loss characteristics on loess slopes covered with aeolian sand layers of different thicknesses under simulated rainfall. J. Hydrol. 549, 244–251.
Zhang, J.Q., Yang, M.Y., Zhang, F.B., Zhang, W., Zhao, T.Y., Li, Y.Y., 2017. Fingerprinting sediment sources after an extreme rainstorm event in a small catchment on the Loess Plateau, China. Land Degrad. Dev. 28, 2527–2539.
Zhang, J.Q., Yang, M.Y., Sun, X.J., Zhang, F.B., 2018. Estimation of wind and water erosion based on slope aspects in the crisscross region of the Chinese Loess Plateau. J. Soils Sediments 18, 1620–1631.
Zhao, G.J., Kondolf, G.M., Mu, X.M., Han, M.W., He, Z., Zan, R.B., Wang, F., Gao, P., Sun, W.Y., 2017. Sediment yield reduction associated with land use changes and check dams in a catchment of the Loess Plateau, China. Catena 148, 126–137.
Zhao, T.Y., Yang, M.Y., Walling, D.E., Zhang, F.B., Zhang, J.Q., 2017. Using check dam deposits to investigate recent changes in sediment yield in the Loess Plateau, China. Glob. Planet. Chang. 152, 88–98.